Measurements of cross sections and oscillator strengths by electron impact for the 5*d* and 7*s* levels of Xe

T. Y. Suzuki, H. Suzuki, F. J. Currell, and S. Ohtani
Institute for Laser Science, University of Electro-Communications, Chofugaoka 1-5-1, Chofu-Shi, Tokyo 182, Japan

T. Takayanagi and K. Wakiya
Department of Physics, Sophia University, Kioicho 7-1, Chiyoda-ku, Tokyo 102, Japan
(Received 28 December 1995)

Differential cross sections and generalized oscillator strengths have been measured for two optically allowed transitions $5p^6(^1S_0)\rightarrow 5p^5(^2P_{3/2})5d(K=\frac{3}{2},J=1)$ and $5p^6(^1S_0)\rightarrow 5p^5(^2P_{3/2})7s(K=\frac{3}{2},J=1)$ and two optically forbidden transitions $5p^6(^1S_0)\rightarrow 5p^5(^2P_{3/2})5d(K=\frac{7}{2},J=3)$ and $5p^6(^1S_0)\rightarrow 5p^5(^2P_{3/2})5d(K=5/2, J=3)$ in Xe by means of electron-energy-loss spectroscopy. These measurements are carried out for electron kinetic energies of 400 and 500 eV at small scattering angles (θ=1.4°–15.1°). Optical oscillator strengths have been determined by extrapolating the generalized oscillator strengths to zero momentum transfer, as (0.298 $\pm$0.045) and (0.0738$\pm$0.011), for the $5p^5(^2P_{3/2})5d(K=\frac{3}{2},J=1)$ and $5p^5(^2P_{3/2})7s(K=\frac{3}{2},J=1)$ states, respectively. Integrated cross sections have also been determined for each impact energy. The errors are estimated to be less than 15%. [S1050-2947(96)09705-3]

PACS number(s): 34.80.Dp

I. INTRODUCTION

We have been continuing a series of measurements of differential cross sections (DCS's) and generalized oscillator strengths (GOS's) for the electron-impact excitation of the resonance lines in rare-gas atoms (Ne,Ar,Kr,Xe). As an addition to the previous measurements of $5p\rightarrow 6s$ transitions in Xe, we present the cross sections and oscillator strengths for $5p\rightarrow 5d,7s$ transitions in Xe. The peaks of the energy-loss spectra corresponding to these states do not contain contributions from other states. As a result, the measurements presented represent these features uncontaminated by the effects of other states. It is especially important to know excitation cross sections for the $5p^5(^2P_{3/2})5d(K=\frac{3}{2},J=1)$ state for some applications because they have the largest values of all excitation cross sections in Xe at high impact energies. Some earlier results of measurements for resonance lines of rare-gas atoms have already been published [1–4].

Few theoretical calculations are available for the *e*-Xe inelastic scattering processes which we are concerned with. Ganas and Green [5] reported a calculation of integrated cross sections (ICS's) for the $5p\rightarrow ns$ transitions with an independent particle model. As for experimental studies, inelastic DCS's and the ICS's were given at 15-, 20-, 30-, and 80-eV impact energies by Filipovic *et al.* [6], and at 20 eV by Williams, Trajmar, and Kupperman [7]. Some preliminary results for the $5p\rightarrow 7s$ transition were reported by Nishimura, Danjo, and Matsuda [8].

We measured DCS's and GOS's for the $5p^5(^2P_{3/2})6s(K=\frac{3}{2},J=1)$ and $5p^5(^2P_{1/2})6s(K=\frac{1}{2},J=1)$ states in a preceding work. In the present work, DCS's and GOS's for optically allowed $5p^5(^2P_{3/2})5d(K=\frac{3}{2},J=1)$ and $5p^5(^2P_{3/2})7s(K=\frac{3}{2},J=1)$ states and optically forbidden $5p^5(^2P_{3/2})5d(K=\frac{7}{2},J=3)$ and $5p^5(^2P_{3/2})5d(K=\frac{5}{2},J=3)$ states, which are designated as $5d[\frac{3}{2}]^0_1$, $7s[\frac{3}{2}]^0_1$, $5d[\frac{7}{2}]^0_3$, $5d[\frac{5}{2}]^0_3$ according to the *J*-1 coupling notation [9], respectively, are measured at 400- and 500-eV impact energies by means of electron-energy-loss spectroscopy (EELS). In *J*-1 coupling, the total angular momentum *J* of the parent ion and the orbital angular momentum 1 of the external electron are coupled. This coupling causes a resultant angular momentum *K*. In turn *K* is coupled with the spin angular momentum of the electron, and causes the resultant *J* value. The $5d[\frac{7}{2}]^0_3$ and $5d[\frac{5}{2}]^0_3$ states have the same angular momentum quantum numbers except for *K* values. The optical oscillator strengths (OOS's) and ICS's are determined from the GOS's, and are compared with the results of calculations and other measurements.

II. EXPERIMENTAL PROCEDURES

The experimental apparatus has been described in preceding papers [1–3]. The electron spectrometer consists of an electron gun, a hemispherical electrostatic energy selector and an energy analyzer, an electron lens system, and an electron detecting system. In this work, the typical energy resolution of the apparatus is 50-meV full width at half maximum (FWHM), and the angular resolution is 0.4° (FWHM).

The relative scattering intensities associated with respective scattering processes were determined from the corresponding peak areas of the energy-loss spectra. Then the absolute DCS's were determined from the relationship

$$\left|\frac{d\sigma}{d\Omega}\right|_{\text{inel}} \Big/ \left|\frac{d\sigma}{d\Omega}\right|_{\text{el}} = \frac{I_{\text{inel}}}{I_{\text{el}}}, \tag{1}$$

where *I* is the scattering intensity, and ''inel'' and ''el'' denote inelastic and elastic scattering, respectively. The influences of the chromatic aberration to the scattering intensities are negligibly small because the impact energies are much

larger than the $5p \rightarrow 5d,7s$ excitation energies. The actual zero-scattering angle has been calibrated using the symmetry of the intensity ratio $I_{\text{inel}}/I_{\text{el}}$ around 0°. $(d\sigma/d\Omega)_{\text{el}}$ was obtained by a calculation using a fitting function, which was based on experimental data of the absolute elastic-scattering cross sections measured by Bromberg [10] and Jansen and de Heer [11]. Using Eq. (1), $(d\sigma/d\Omega)_{\text{inel}}$ can be determined by multiplying the intensity ratio by the factor $(d\sigma/d\Omega)_{\text{el}}$.

The GOS $F(K)$ is calculated from the equation [12]

$$F(K)=\frac{W}{2}\frac{k_i}{k_f}K^2\left(\frac{d\sigma}{d\Omega}\right), \tag{2}$$

where W is the excitation energy, k_i and k_f are the momenta of the colliding electrons before and after collision, and K is the magnitude of the momentum-transfer vector. All quantities are in atomic units.

The limiting value of the GOS as K^2 approaches zero gives the OOS whether the Born approximation is valid or not. In order to obtain the OOS, we have extrapolated the experimental GOS values to zero momentum transfer using the least-squares method with polynomials of the form [13]

$$F(K)=\frac{1}{(1+x^2)^l}\left[f_0+\sum_{n=1}^{m} f_n\left(\frac{x^2}{1+x^2}\right)^n\right], \tag{3}$$

where $l=6$ for the $5p \rightarrow 7s$ transition, $l=8$ for the $5p \rightarrow 5d$ transitions, f_0 is the OOS, and f_n are the coefficients which describe the relation of F to K. X is equal to K/Y, and Y is equal to $\sqrt{2I}+\sqrt{2(I-W)}$. I and W are the ionization energy and excitation energy, respectively.

Recently, another extrapolation formula for optically allowed transitions was constructed by Msezane and Sakmar [14] considering the rigorous physical domain on K^2. It gives the behavior of the GOS in the vicinity of $K=0$. The formula is expressed as

$$F(K)=-f_0\left(1-\frac{2}{\left(1+\frac{K^2}{2W}\right)}\right). \tag{4}$$

It has been shown that Eq. (4) agrees well with the experimental results for small K^2 ($\leqslant$0.05 a.u.) [15]. We compare our results with the values given from the formula in Sec. III.

Employing either (2) or (3), the ICS σ is obtained as follows:

$$\sigma=\frac{4\pi}{Wk_i^2}\int_{k_i-k_f}^{k_i+k_f}\frac{F(K)}{K}\,dK. \tag{5}$$

We have made numerical calculations of the ICS in the Born approximation according to this equation.

III. RESULTS AND DISCUSSION

Typical energy-loss spectra are shown in Fig. 1. These spectra were taken at an impact energy of 500 eV and scattering angles of 1.9° and 5.1°. The energy-loss peaks have been identified by comparing them with the spectroscopic values of the transition energy table compiled by Moore [9].

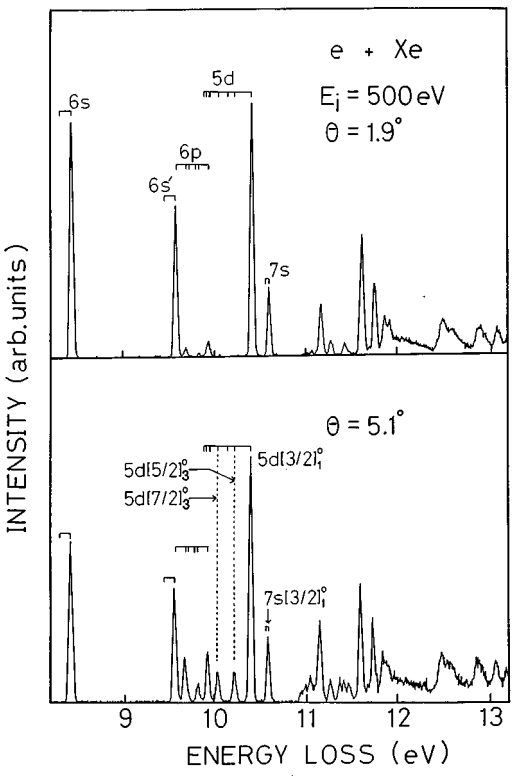

FIG. 1. Typical electron-energy-loss spectra of Xe, for 500-eV impact energy at the scattering angles of 1.9° and 5.1°.

The most intense peak at 10.401 eV corresponds to the excitation to the $5d[\frac{3}{2}]^0_1$ state from the ground state. Adjacent peaks at 10.593, 10.039, and 10.220 eV correspond to excitation to the $7s[\frac{3}{2}]^0_1$, $5d[\frac{7}{2}]^0_3$, and $5d[\frac{5}{2}]^0_3$ states, respectively. The $5d[\frac{7}{2}]^0_3$ and $5d[\frac{5}{2}]^0_3$ peaks are well separated from neighboring states. The intensity ratios of the $5d[\frac{3}{2}]^0_1$, $7s[\frac{3}{2}]^0_1$, $5d[\frac{7}{2}]^0_3$, and $5d[\frac{5}{2}]^0_3$ peaks to the elastic-scattering intensity are given in Table I.

The absolute elastic-scattering cross sections were obtained using a fit to the measurements of Bromberg [10] and Jansen and de Heer [11]. It is known that a curve of a semilogarithmic plot of $(d\sigma/d\Omega)_{\text{el}}$ against K shows a linear behavior in the range of small K. The elastic-scattering cross sections are fitted to the equation

$$\ln\left(\frac{d\sigma}{d\Omega}\right)_{\text{el}}=c_0+c_1K+c_2K^2+c_3K^3, \tag{6}$$

where c_0, c_1, c_2, and c_3 are the fitting parameters. Numerical results of $(d\sigma/d\Omega)_{\text{el}}$ are listed in Table I.

DCS's for the $5d[\frac{3}{2}]^0_1$ and $7s[\frac{3}{2}]^0_1$ excitation for impact energies of 400 and 500 eV are shown in Fig. 2 as functions of the scattering angle. The DCS's for both excitations have the same forward-peaking angular dependence as those for the $6s[\frac{3}{2}]^0_1$ and $6s[\frac{1}{2}]^0_1$ we measured before [3], and possess shallow minima except for that of the $5d[\frac{3}{2}]^0_1$ excitation at 500 eV.

The DCS's for the $5d[\frac{7}{2}]^0_3$ and $5d[\frac{5}{2}]^0_3$ excitations are shown in Fig. 3 as functions of the scattering angle. It is

TABLE I. The intensity ratios $(d\sigma/d\Omega)_{\text{inel}}/(d\sigma/d\Omega)_{\text{el}}$ and the DCS's $(d\sigma/d\Omega)_{\text{inel}}$ (in atomic units) for excitation of the $5d[3/2]_1^0$, $7s[3/2]_1^0$, $5d[7/2]_3^0$, and $5d\ [5/2]_3^0$ states at impact energies of 400 and 500 eV. The absolute elastic differential cross sections $(d\sigma/d\Omega)_{\text{el}}$, are also listed. The numbers in brackets denote powers of 10. The $(d\sigma/d\Omega)_{\text{el}}$ are obtained by the interpolation and extrapolation of the results of Bromberg [10] and Jansen and de Heer [11].

Angle (deg)	$(d\sigma/d\Omega)_{\text{el}}$ (a_0^2/sr)	Intensity ratio $5d[\frac{3}{2}]_1^0$	Intensity ratio $7s[\frac{3}{2}]_1^0$	$(d\sigma/d\Omega)_{\text{inel}}$ (a_0^2/sr) $5d[\frac{3}{2}]_1^0$	$(d\sigma/d\Omega)_{\text{inel}}$ (a_0^2/sr) $7s[\frac{3}{2}]_1^0$
		400 eV			
1.4	1.68[2]	3.57[−1]	9.21[−2]	5.98[1]	1.55[1]
1.9	1.49[2]	2.35[−1]	6.07[−2]	3.50[1]	9.04
2.4	1.33[2]	1.53[−1]	4.06[−2]	2.04[1]	5.42
2.9	1.20[2]	1.08[−1]	2.85[−2]	1.30[1]	3.42
3.6	1.05[2]	6.70[−2]	1.90[−2]	7.01	1.99
4.1	9.50[1]	4.85[−2]	1.48[−2]	4.61	1.40
4.6	8.64[1]	3.38[−2]	1.01[−2]	2.92	8.75[−1]
5.1	7.84[1]	2.64[−2]	7.97[−3]	2.07	6.25[−1]
5.6	7.11[1]	1.68[−2]	5.04[−3]	1.20	3.59[−1]
6.1	6.44[1]	1.30[−2]	3.63[−3]	8.34[−1]	2.34[−1]
7.1	5.24[1]	7.10[−3]	1.88[−3]	3.72[−1]	9.83[−2]
8.1	4.22[1]	3.62[−3]	8.88[−4]	1.53[−1]	3.75[−2]
9.1	3.37[1]	2.36[−3]	5.29[−4]	7.93[−2]	1.78[−2]
10.1	2.67[1]	2.14[−3]	4.67[−4]	5.71[−2]	1.25[−2]
11.1	2.12[1]	1.97[−3]	5.38[−4]	4.19[−2]	1.14[−2]
12.1	1.69[1]	1.80[−3]	6.79[−4]	3.04[−2]	1.15[−2]
13.1	1.36[1]	2.37[−3]	9.59[−4]	3.23[−2]	1.31[−2]
14.1	1.11[1]	2.73[−3]	9.04[−4]	3.02[−2]	1.00[−2]
15.1	9.17	2.44[−3]	8.80[−4]	2.24[−2]	8.07[−3]
		500 eV			
1.4	1.60[2]	3.14[−1]	8.05[−2]	5.04[1]	1.29[1]
1.9	1.43[2]	1.99[−1]	5.07[−2]	2.84[1]	7.24
2.4	1.28[2]	1.27[−1]	3.36[−2]	1.63[1]	4.30
2.9	1.16[2]	8.28[−2]	2.19[−2]	9.59	2.54
3.6	1.01[2]	4.97[−2]	1.37[−2]	5.04	1.39
4.1	9.23[1]	3.41[−2]	9.95[−3]	3.15	9.18[−1]
4.6	8.40[1]	2.16[−2]	6.22[−3]	1.81	5.22[−1]
5.1	7.63[1]	1.60[−2]	4.70[−3]	1.22	3.59[−1]
5.6	6.92[1]	1.09[−2]	3.31[−3]	7.53[−1]	2.29[−1]
6.1	6.25[1]	7.92[−3]	2.27[−3]	4.95[−1]	1.42[−1]
7.1	5.05[1]	3.97[−3]	1.01[−3]	2.00[−1]	5.11[−2]
8.1	4.02[1]	2.31[−3]	4.52[−4]	9.28[−2]	1.82[−2]
9.1	3.17[1]	1.77[−3]	3.71[−4]	5.60[−2]	1.17[−2]
10.1	2.48[1]	1.56[−3]	4.42[−4]	3.87[−2]	1.10[−2]
11.1	1.94[1]	1.56[−3]	6.35[−4]	3.03[−2]	1.23[−2]
12.1	1.53[1]	1.70[−3]	6.16[−4]	2.60[−2]	9.41[−3]
13.1	1.22[1]	1.85[−3]	7.54[−4]	2.25[−2]	9.17[−3]
14.1	9.84	1.68[−3]	6.18[−4]	1.65[−2]	6.08[−3]

Angle (deg)	$(d\sigma/d\Omega)_{\text{el}}$ (a_0^2/sr)	Intensity ratio $5d[\frac{7}{2}]_3^0$	Intensity ratio $5d[\frac{5}{2}]_3^0$	$(d\sigma/d\Omega)_{\text{inel}}$ (a_0^2/sr) $5d[\frac{7}{2}]_3^0$	$(d\sigma/d\Omega)_{\text{inel}}$ (a_0^2/sr) $5d[\frac{5}{2}]_3^0$
		400 eV			
2.4	1.33[2]	1.03 [−3]	1.56[−3]	1.38[−1]	2.08[−1]
2.9	1.20[2]	1.32 [−3]	1.52[−3]	1.59[−1]	1.82[−1]
3.6	1.05[2]	1.50 [−3]	1.80[−3]	1.57[−1]	1.88[−1]
4.1	9.50[1]	1.74[−3]	1.89[−3]	1.65[−1]	1.79[−1]
4.6	8.64[1]	1.69[−3]	2.21[−3]	1.46[−1]	1.91[−1]
5.1	7.84[1]	2.11[−3]	2.25[−3]	1.65[−1]	1.77[−1]
5.6	7.11[1]	2.31[−3]	2.35[−3]	1.65[−1]	1.67[−1]
6.1	6.44[1]	2.55[−3]	2.56[−3]	1.64[−1]	1.65[−1]
7.1	5.24[1]	2.76[−3]	2.82[−3]	1.44[−1]	1.47[−1]
8.1	4.22[1]	2.76[−3]	2.60[−3]	1.16[−1]	1.10[−1]
9.1	3.37[1]	2.95[−3]	3.01[−3]	9.94[−2]	1.01[−1]

TABLE I. (*Continued*).

Angle (deg)	$(d\sigma/d\Omega)_{el}$ (a_0^2/sr)	Intensity ratio $5d[\frac{7}{2}]^0_3$	Intensity ratio $5d[\frac{5}{2}]^0_3$	$(d\sigma/d\Omega)_{inel}$ (a_0^2/sr) $5d[\frac{7}{2}]^0_3$	$(d\sigma/d\Omega)_{inel}$ (a_0^2/sr) $5d[\frac{5}{2}]^0_3$
		400 eV			
10.1	2.67[1]	2.97[−3]	2.96 [−3]	7.95 [−2]	7.92 [−2]
11.1	2.12[1]	3.02[−3]	2.51 [−3]	6.41 [−2]	5.33 [−2]
12.1	1.69 [1]	2.49[−3]	2.43 [−3]	4.22 [−2]	4.11 [−2]
13.1	1.36[1]	2.65[−3]	2.48 [−3]	3.61 [−2]	3.38 [−2]
14.1	1.11[1]	2.34[−3]	2.38 [−3]	2.59 [−2]	2.64 [−2]
15.1	9.17	2.11[−3]	1.89 [−3]	1.94 [−2]	1.73 [−2]
		500 eV			
2.4	1.28 [2]	1.28[−3]	1.73 [−3]	1.64 [−1]	2.22 [−1]
2.9	1.16 [2]	1.35[−3]	1.63 [−3]	1.56 [−1]	1.88 [−1]
3.6	1.01 [2]	1.60[−3]	1.68 [−3]	1.62 [−1]	1.71 [−1]
4.1	9.23 [1]	1.74[−3]	1.74 [−3]	1.60 [−1]	1.60 [−1]
4.6	8.40 [1]	2.07[−3]	2.04 [−3]	1.73 [−1]	1.71 [−1]
5.1	7.63 [1]	2.16[−3]	2.04 [−3]	1.65 [−1]	1.56 [−1]
5.6	6.92 [1]	2.63[−3]	2.44 [−3]	1.82 [−1]	1.69 [−1]
6.1	6.25 [1]	2.47[−3]	2.34 [−3]	1.54 [−1]	1.47 [−1]
7.1	5.05 [1]	2.62[−3]	2.48 [−3]	1.33 [−1]	1.25 [−1]
8.1	4.02 [1]	2.60[−3]	2.76 [−3]	1.05 [−1]	1.11 [−1]
9.1	3.17 [1]	2.69[−3]	2.28 [−3]	8.52 [−2]	7.22 [−2]
10.1	2.48 [1]	2.54[−3]	2.56 [−3]	6.29 [−2]	6.36 [−2]
11.1	1.94 [1]	2.14[−3]	2.00 [−3]	4.15 [−2]	3.89 [−2]
12.1	1.53 [1]	1.82[−3]	1.69 [−3]	2.78 [−2]	2.58 [−2]
13.1	1.22 [1]	1.71[−3]	1.64 [−3]	2.07 [−2]	1.99 [−2]
14.1	9.84	1.21[−3]	1.58 [−3]	1.19 [−2]	1.56 [−2]

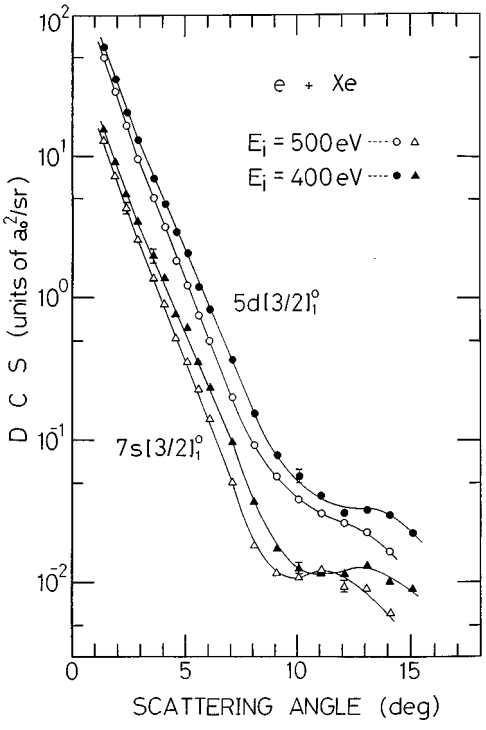

FIG. 2. Differential cross sections for the excitation of the $5d[\frac{3}{2}]^0_1$ (circles) and $7s[\frac{3}{2}]^0_1$ (triangles) states in Xe as a function of the scattering angle.

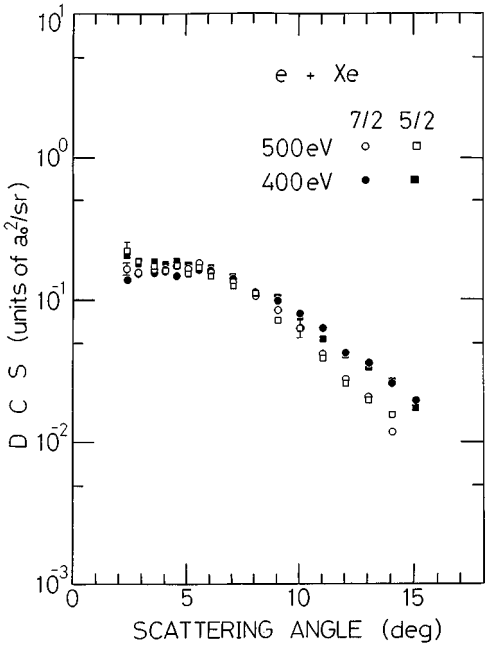

FIG. 3. Differential cross sections for the excitation of the $5d[\frac{7}{2}]^0_3$ and $5d[\frac{5}{2}]^0_3$ states in Xe as a function of the scattering angle.

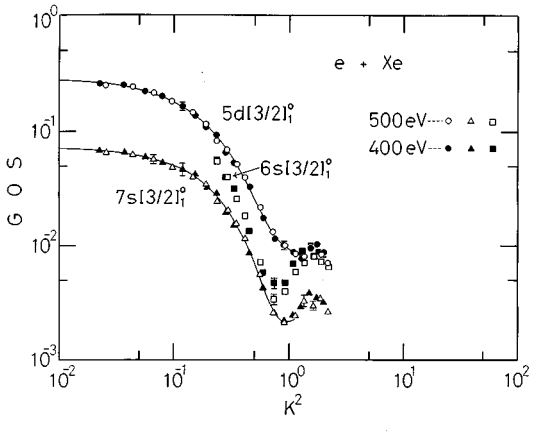

FIG. 4. The generalized oscillator strengths for the excitation of the $5d[\frac{3}{2}]_1^0$ (circles) and $7s[\frac{3}{2}]_1^0$ (triangles) states in Xe as a function of the squared momentum transfer K^2 (log-log plots). The squares are part of the $6s[\frac{3}{2}]_1^0$ data remeasured. The solid lines are fitted lines using Eq. (3).

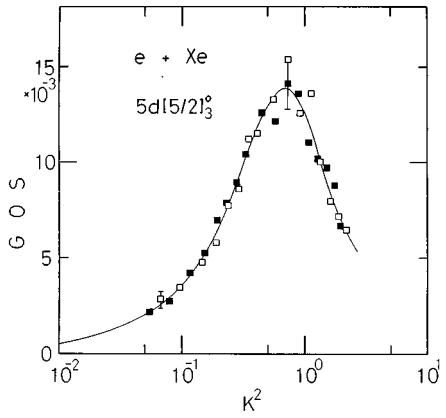

FIG. 6. The generalized oscillator strengths for the excitation of the $5d[\frac{5}{2}]_3^0$ state in Xe as a function of the squared momentum transfer K^2 (semilog plots). The open squares are the values at 500 eV, and the closed squares those at 400 eV. The solid lines are fitted lines using Eq. (3).

found that the DCS's for both excitations have a flat angular dependence and show little impact energy dependence in a region of the scattering angle smaller than about 8°. In a region larger than about 6°, both DCS's show an angular dependence more gentle than those for the $5d[\frac{3}{2}]_1^0$ and $7s[\frac{3}{2}]_1^0$ excitations. No difference in the values of the DCS's for the $5d[\frac{7}{2}]_3^0$ and $5d[\frac{5}{2}]_3^0$ excitations has been observed in the region covered by our experiment. For lower electron-impact energies [6,7], it was reported that DCS's for the $5d[\frac{7}{2}]_3^0$ excitation are larger than those for the $5d[\frac{5}{2}]_3^0$ excitation.

The GOS's for the $5d[\frac{3}{2}]_1^0$ and $7s[\frac{3}{2}]_1^0$ excitation processes are derived from the DCS's using Eq. (2), and are shown in Fig. 4. The DCS's for the $6s[\frac{3}{2}]_1^0$ excitation have been remeasured, and the GOS's around the minimum are also shown in Fig. 4. The GOS's for the $5d[\frac{7}{2}]_3^0$ and $5d[\frac{5}{2}]_3^0$ excitations are also shown in Figs. 5 and 6, respectively. In the graph of the GOS against K^2, the data points for the $5d[\frac{3}{2}]_1^0$ and $7s[\frac{3}{2}]_1^0$ excitations taken at 400 and 500 eV lie on the same curves in the region $K^2<1.5$. These GOS curves show minima like those for $6s[\frac{3}{2}]_1^0$ [3]. However the GOS's for $5d[\frac{3}{2}]_1^0$ do not have a minimum as deep as those for $6s[\frac{3}{2}]_1^0$, and the GOS's for $7s[\frac{3}{2}]_1^0$ do not have an impact energy dependence in the vicinity of K^2, for which the GOS has its minimum value. The apparent GOS's remeasured for $6s[\frac{3}{2}]_1^0$ around the minimum were found to increase as the impact energy decreases. If the radial Hartree-Fock wave function of the $7s[\frac{3}{2}]_1^0$ state had its most prominent maximum beyond the outermost node like that of $6s[\frac{3}{2}]_1^0$, the GOS's around the minimum would have an energy dependence because of effects not included in the first Born approximation (see Ref. [16]). We thus suggest that the radial wave function of the $7s[\frac{3}{2}]_1^0$ state has a different form from that of the $6s[\frac{3}{2}]_1^0$ wave function. As for $5d[\frac{7}{2}]_3^0$ and $5d[\frac{5}{2}]_3^0$ excitations, it seems that the data points of the GOS's taken at 400 and 500 eV lie on the same

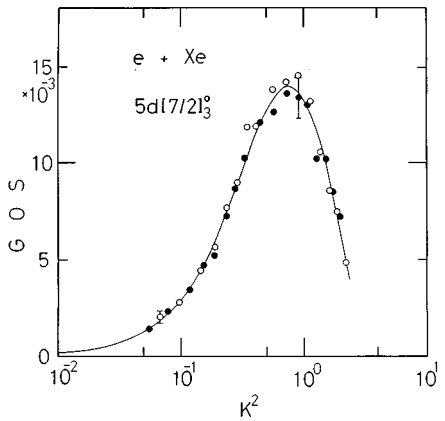

FIG. 5. The generalized oscillator strengths for the excitation of the $5d[\frac{7}{2}]_3^0$ state in Xe as a function of the squared momentum transfer K^2 (semilog plots). The open circles are the values at 500 eV, and the closed circles those at 400 eV. The solid lines are fitted lines using Eq. (3).

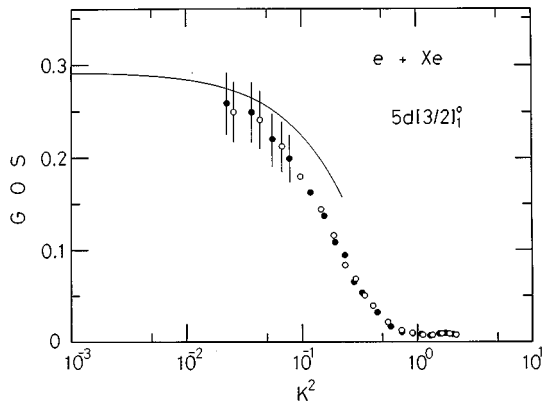

FIG. 7. A comparison of the present generalized oscillator strengths for the $5d[\frac{3}{2}]_1^0$ state with the formula recommended by Msezane and Sakmar (Ref. [14]). The OOS value used is determined by the extrapolation using Eq. (3). The solid line is calculated by Eq. (4). The other symbols are the same as in Fig. 4.

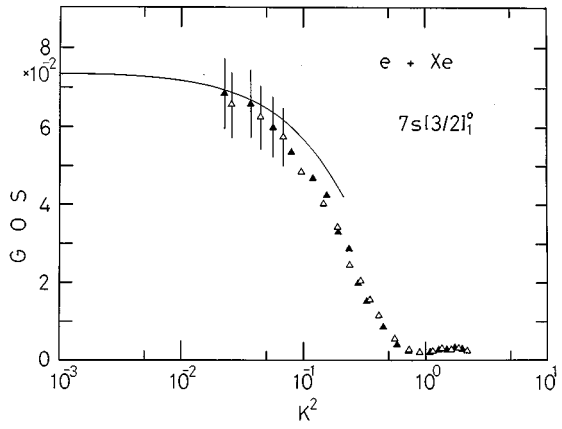

FIG. 8. A comparison of the present generalized oscillator strengths for the $7s[\frac{3}{2}]_1^0$ state with the values of a formula Eq. (4). The solid line is calculated by Eq. (4). The other symbols are the same as in Fig. 4.

TABLE II. Comparisons of the present optical oscillator strengths for the $5d[\frac{3}{2}]_1^0$ and $7s[\frac{3}{2}]_1^0$ states in Xe with those of other authors.

Author	OOS $5d[\frac{3}{2}]_1^0$	OOS $7s[\frac{3}{2}]_1^0$	Ratio of the OOS's $7s[\frac{3}{2}]_1^0/5d[\frac{3}{2}]_1^0$
		EELS	
This work	0.298±0.045	0.0738±0.011	0.248
Lu[a]	0.381	0.09	0.236
Delage[b]	0.395±0.158	0.11±0.044	0.278
J. Geiger[c]	0.395	0.0968	0.245
W. F. Chan[d]	0.379±0.019	0.0859±0.0043	0.227
		Optical measurements	
W. R. Ferrell[e]	0.370±0.07	0.088±0.01	0.238
S. D. Kramer[f]		0.098±0.012	
		Theory	
Geiger[c]	0.550	0.0769	0.140

[a]Reference [18] (low-energy electron impact).
[b]Reference [19] (low-energy electron impact).
[c]Reference [20] (high-energy electron impact, energy-dependent quantum defect theory).
[d]Reference [21] [high resolution dipole (e,e) method].
[e]Reference [22] (optical phase matching).
[f]Reference [23] (optical phase matching).

TABLE III. Integrated cross sections for the excitation of the $5d[\frac{3}{2}]_1^0$ and $7s[\frac{3}{2}]_1^0$ states in Xe.

Impact energy (eV)	Cross section (10^{-17} cm^2) $5d[3/2]_1^0$	$7s[3/2]_1^0$
400	1.48±0.22	0.378±0.057
500	1.26±0.19	0.323±0.048

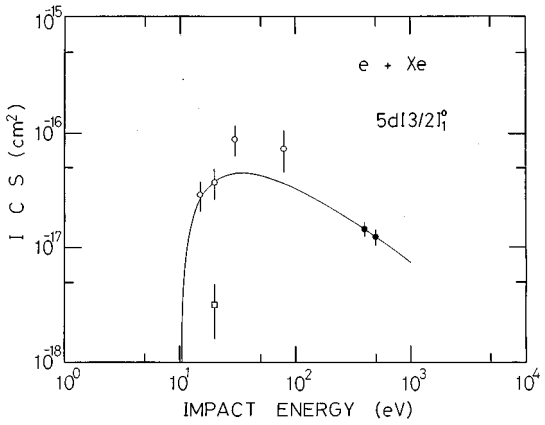

FIG. 9. Integrated cross sections for the excitation of the $5d[\frac{3}{2}]_1^0$ state in Xe as a function of the impact energy. The solid circles are the present results, and the solid curve is drawn by extrapolation to the lower impact energies within the framework of the Born approximation using Eq. (5). The open circles are experimental results of Filipovic *et al.* (Ref. [6]), and the open rectangle is by Williams, Trajmar, and Kuppermann (Ref. [7]).

curves over the whole range of K^2 measured, although the data around the maxima are scattered a little.

Comparisons of the present GOS's for the $5d[\frac{3}{2}]_1^0$ and $7s[\frac{3}{2}]_1^0$ transitions with the values of a formula recommended by Msezane and Sakmar [14] are shown in Figs. 7 and 8. Both of our GOS's agree with their curves at small K^2 ($\leqslant 0.05$) within the experimental errors.

The present results of the OOS's and the ratios of the OOS for $7s[\frac{3}{2}]_1^0$ to $5d[\frac{3}{2}]_1^0$ are compared with the published data in Table II. The present results of the OOS's appear to be smaller than other experimental values by 20–25 %. However, there is not much difference between our ratio of the $7s[\frac{3}{2}]_1^0/5d[3/2]_1^0$ OOS's and some other experimental ones. The question may be how to determine the absolute values, or how to extrapolate the GOS values. It was found that our previous $6s[3/2]_1^0$ DCS's gave very good agreement with the values calculated by the relativistic distorted-wave method [17] published after our previous paper. We found

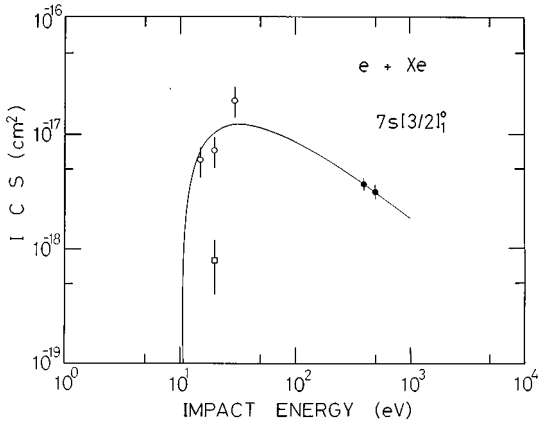

FIG. 10. Integrated cross sections for the excitation of the $7s[\frac{3}{2}]_1^0$ state in Xe as a function of the impact energy. The same symbols and notations are used as in Fig. 9.

that DCS's remeasured for $6s[\frac{3}{2}]_1^0$ agreed well with our previous data. Our extrapolation procedure seems to be reasonable according to Figs. 7 and 8. Considering these facts, we suggest that although our OOS's are smaller than other experimental values, they are a result of the most careful practice of the intermediate-energy electron-energy-less spectroscopy (EELS) method for the OOS measurement.

The ICS's for the $5d[\frac{3}{2}]_1^0$ and $7s[\frac{3}{2}]_1^0$ excitations at 400- and 500-eV impact energies are determined using Eq. (5), and are tabulated in Table III. ICS's at lower impact energies can be calculated from the GOS's at 400 and 500 eV within the framework of the Born approximation. These results are shown in Figs. 9 and 10, where experimental values measured by Williams, Trajmar, and Kuppermann [7] and Filipovic *et al.* [6] are also presented for comparison. Considering that cross sections calculated according to the Born approximation are larger at lower impact energies than experimental ones, provided no local effects such as resonances produce an enhancement, the results of Filipovic *et al.* at 15 and 20 eV seem to be reasonable. The ICS's for both the $5d[\frac{3}{2}]_1^0$ and $7s[\frac{3}{2}]_1^0$ transitions given by Williams, Trajmar, and Kuppermann are much smaller than those we have measured. As mentioned in a previous paper [3], this discrepancy is considered to be due to their normalization procedure.

Systematic errors in the measured DCS's due to the effect of the limited angular resolution are negligibly small in the present experiment. The errors in the results for DCS's and GOS's are estimated to be 13%, the quadratic sum of the random error to be 10%, the systematic error to be 3%, and the error of the standard elastic-scattering cross section to be 7%. The uncertainties in the OOS are estimated to be 15%, the quadratic sum of the errors of the GOS's to be 13%, and the errors due to the extrapolation procedure of the GOS's to be 8%. The errors in the ICS's are of similar magnitudes.

[1] G. P. Li, T. Takayanagi, K. Wakiya, H. Suzuki, T. Ajiro, S. Yagi, S. S. Kano, and H. Takuma, Phys. Rev. A **38**, 1240 (1988).
[2] T. Takayanagi, G. P. Li, K. Wakiya, H. Suzuki, T. Ajiro, T. Inaba, S. S. Kano, and H. Takuma, Phys. Rev. A **41**, 5948 (1990).
[3] T. Y. Suzuki, Y. Sakai, B. S. Min, T. Takayanagi, K. Wakiya, H. Suzuki, T. Inaba, and H. Takuma, Phys. Rev. A **43**, 5867 (1991).
[4] T. Y. Suzuki, H. Suzuki, S. Ohtani, B. S. Min, T. Takayanagi, and K. Wakiya, Phys. Rev. A **49**, 4578 (1994).
[5] P. S. Ganas and A. E. S. Green, Phys. Rev. A **4**, 182 (1971).
[6] D. Filipovic, B. Marinkovic, V. Pejcev, and L. Vuskovic, Phys. Rev. A **37**, 356 (1988).
[7] W. Williams, S. Trajmar, and A. Kuppermann, J. Chem. Phys. **62**, 3031 (1975).
[8] H. Nishimara, A. Danjo, and T. Matsuda, in *Abstracts of Contributed Papers of the Fourteenth International Conference on the Physics of Electronic and Atomic Collisions, Palo Alto, 1985*, edited by M. J. Coggiola, D. L. Huestis, and R. P. Saxon (ICPEAC, Palo Alto, 1985), p. 108.
[9] C. E. Moore, *Atomic Energy Levels*, Natl. Bur. Stand. (U.S.) Circ. No. 467 (U.S. GPO, Washington, D.C., 1958), Vol. III.
[10] J. P. Bromberg, J. Chem. Phys. **61**, 963 (1974).
[11] R. H. J. Jansen and F. J. de Heer, J. Phys. B **9**, 213 (1976).
[12] H. Bethe, Ann. Phys. (Leipzig) **5**, 325 (1930).
[13] K. N. Klump and E. N. Lassettre, J. Chem. Phys. **68**, 886 (1978).
[14] A. Z. Msezane and I. A. Sakmar, Phys. Rev. A **49**, 2405 (1994).
[15] See, for example, A. Z. Msezane and Z. Chen, Phys. Rev. A **49**, 3083 (1994).
[16] Y. K. Kim and M. Inokuti, Phys. Rev. Lett. **21**, 1146 (1968).
[17] T. Zuo, R. P. McEachran, and A. D. Stauffer, J. Phys. B **25**, 3393 (1992).
[18] K. T. Lu, Phys. Rev. A **4**, 579 (1971).
[19] A. Delage and J. D. Carette, Phys. Rev. A **14**, 1345 (1976).
[20] J. Geiger, Z. Phys. A **282**, 129 (1977).
[21] W. F. Chan, G. Cooper, X. Guo, G. R. Burton, and C. E. Brion, Phys. Rev. A **46**, 149 (1992).
[22] W. R. Ferrell, M. G. Payne, and W. R. Garrett, Phys. Rev. A **35**, 5020 (1987).
[23] S. D. Kramer, C. H. Chen, and M. G. Payne, Opt. Lett. **9**, 347 (1984).